ADVANCED MATERIALS TECHNOLOGIES
www.advmattechnol.de

Quantitative Assessment of Gut and Vascular Barriers in TTOP, a Cartridge-Based Bicompartmental Culture Platform

*Lorenzo Pietro Coppadoro, Maria Lombardi, Sabrina Nicolò, Alessandra Maria Anna Rando, Gianfranco Beniamino Fiore, Chiara Foglieni, and Monica Soncini**

Bicompartmental in vitro cultures are performed using culture inserts in multi-well plates. The main challenge of these systems is sample retrieval, which potentially impacts the experimental outcomes. To overcome this challenge, we developed a novel cartridge-based device called true-tissue-on-platform (TTOP). Our device offers the same handling than multi-well inserts with a key difference: the cartridge can be easily retrieved and reused without compromising sample morphology. The functionality of TTOP is demonstrated by building gut and vascular barrier in-vitro models. Barrier tightness is assessed by measuring trans epithelial/endothelial electrical resistance (TEER) and permeability by Lucifer Yellow assay (LY). Geometry-related effects on TEER are evaluated using a finite element model, comparing TTOP to conventional inserts, which showed an improvement in data robustness and accuracy. Moreover, the device enabled the detection of inflammation-related changes by comparing untreated versus Tumor-Necrosis-Factor-α-treated cell barriers, revealing significant differences both with TEER and LY assays. Preliminary data on coupled gut/vascular barriers in the two compartments supported the feasibility of mimicking the gut–vascular barrier in vitro. This new cartridge-based concept may provide a simple and modular device, accessible to any biological laboratory, enabling controlled handling of the biological samples during and after the experiment.

1. Introduction

In the human body, many tissues act as compartmental protective barriers contributing to homeostasis through actively regulating the passage of ions, molecules, and pathogens.[1] Among others, the gut–vascular barrier (GVB) determines the intestinal transepithelial absorption of nutrients and drugs, by modulating luminal mucosa permeability, thus the passage into circulation.[2] Alteration in GVB barrier function is closely associated with changes in intercellular tightness (i.e., leakage increase), reflected by changes in the expression of tight junctions (e.g., Zonula Occludens-1, ZO-1[3]) and can lead to the passage of pathogens or to pro-inflammatory activation, leading to pathological conditions (e.g., inflammatory bowel disease, irritable bowel syndrome, and liver disease).[4] In vitro models of the intestinal and vascular barriers have traditionally relied on standard multi-well inserts, such as transwell (TW) systems, to study molecular transport across epithelial and endothelial layers.[5–10] For example, Ayehunie and coworkers[10] developed a primary three-dimensional (3D) organotypic model of the human small intestine in TW that recapitulates its structural features and physiological barrier properties, and expresses key drug transporters and metabolizing enzymes present in the intestinal epithelium. With a similar purpose, Stappenback and colleagues[11] developed a TW based intestinal model starting from patient-specific human enteroids, first disgregated and then seeded on a microporous polymeric membrane. Similarly, Albritton and colleagues[12] slightly modified a conventional TW insert to expose only crypt regions to bicompartmental stimuli, promoting crypt localization in primary organoid-derived monolayers. Mohammadi and coworkers[13] further advanced the field by increasing experimental throughput, developing a 96-well TW system to culture human gut organoids and extract quantitative responses to investigate gut inflammatory responses. However, the intestinal barrier represents a complex multicellular interface that involves a broad range of additional cell types contributing to tissue homeostasis and to host responses against microbial or pharmacological challenges at the epithelial surface. For this reason, current research efforts are increasingly directed toward integrating stromal fibroblasts,[14,15] immune cells,[16–18] or endothelial cells[19,20]

L. P. Coppadoro, A. M. A. Rando, G. B. Fiore, M. Soncini
Department of Electronics, Information and Bioengineering (DEIB)
Politecnico di Milano
Piazza Leonardo da Vinci 32, Milan 20133, Italy
E-mail: monica.soncini@polimi.it
M. Lombardi, S. Nicolò, C. Foglieni
Cardiovascular Research Center
IRCCS San Raffaele Hospital
Via Olgettina, 60, Milan 20132, Italy

The ORCID identification number(s) for the author(s) of this article can be found under https://doi.org/10.1002/admt.202500065

DOI: 10.1002/admt.202500065

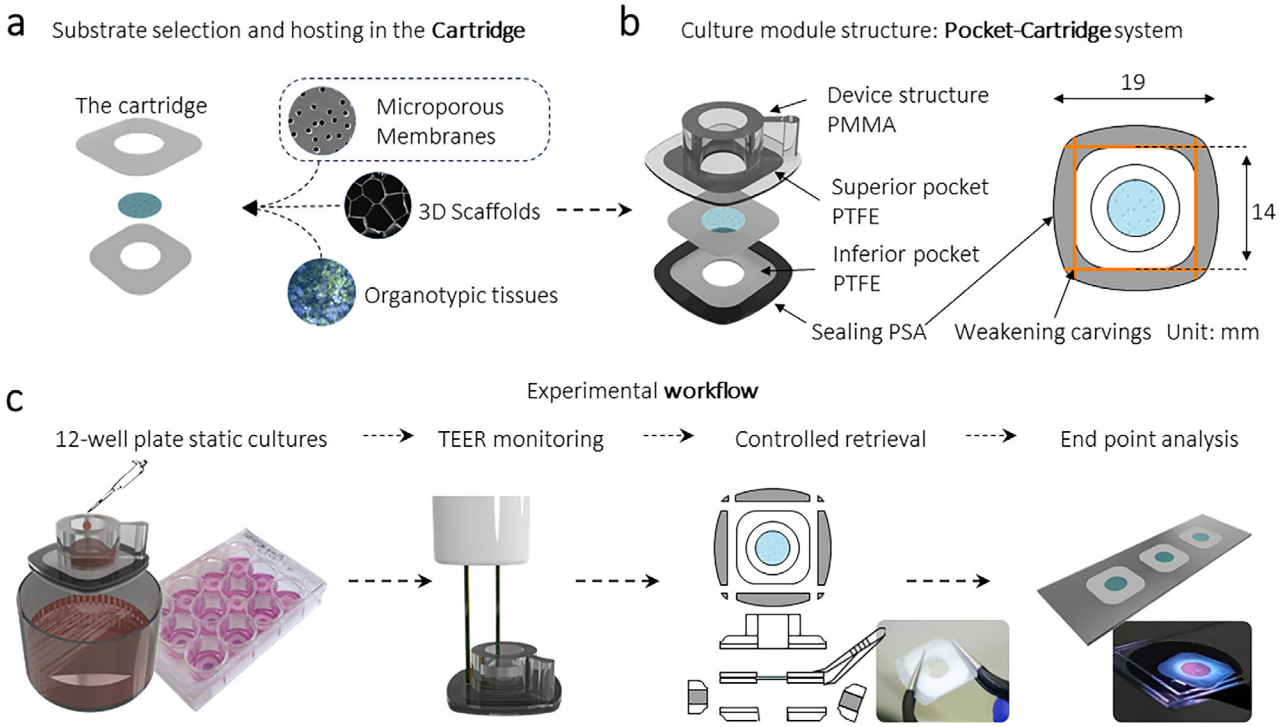

Figure 1. Device overview and workflow. a) TTOP cartridge. The cartridge allows hosting different bidimensional (2D) or 3D structures such as microporous membranes, 3D scaffolds, or commercially available organotypic cultures. b) TTOP pocket-cartridge system. After assembly, the cartridge can be inserted into the culture module forming the so-called pocket-cartridge system. This configuration enables compartmental separation without permanently affixing the cartridge to the module. A double-sided adhesive tape (sealing PSA) is positioned forming a frame around the cartridge, maintaining the hydrophobic layers of the pocket-cartridge system close enough to guarantee compartment separation. Orange lines depict weakening carvings created on the PMMA surface, which allow a simple retrieval procedure. c) Culture module usage procedure. The culture module is positioned in a standard 12-well plate and the two compartments filled with culture medium. Cells are poured on the porous membrane by gravity, thanks to the open-well configuration. During the culture, it is possible to monitor the barrier formation with standard laboratory techniques (e.g., TEER measurements). At the end of the experiment, the cartridge can be retrieved, through a controlled snap-crack breaking of the culture module along the weakening carvings for microscopy imaging or end-point analysis.

populations that better replicate the physiological cross-talks occurring in vivo. While these systems provide valuable insights, they are often hampered in practice by manual handling challenges, being in most cases based on TW systems. In fact, co-culturing cells on the two sides of a TW insert requires good manual skills, since the process typically involves flipping the inserts, placing a small drop of medium containing cells on the basal side of the membrane, and keeping them under a biological hood until the cells attach, as the inserts do not fit the multi-well plate in the flipped position.[16–18,21–23] Furthermore, retrieving biological samples from TW inserts without damaging tissue morphology remains a critical bottleneck, requiring scalpel blades or punchers, hence making careful handling crucial to prevent any damage to the sample. Moreover, commercially available TW inserts typically incorporate microporous polymeric membranes, which can limit direct physical contact between co-cultured cells and provide a rigid substrate that poorly represents the native intestinal extracellular matrix (ECM). To address these limitations, Hinman and colleagues[18] engineered custom TW systems containing macrogrids of woven polyester strands supporting a 3D collagen I hydrogel, thereby enabling cell migration and providing a softer substrate for cell growth. Similarly, Darling and colleagues[14] utilized commercially available highly porous 3D scaffolds (Alvetex) to establish a subepithelial stromal compartment enriched with fibroblasts, allowing the study of direct contact co-culture effects. However, these approaches remain largely confined to a few bioengineering laboratories where TW customization or device development is feasible, as they typically require access to design tools, rapid prototyping technologies, and specialized expertise. Therefore, there is a need for standardized and versatile systems that can overcome the limitations of TW inserts while being readily adoptable by laboratories without specialized engineering expertise. With this goal in mind, we developed a standardized, modular, and versatile device, named true-tissue-on-platform (TTOP), for the realization of bicompartmental in vitro cultures/co-cultures of tissue barriers. TTOP consists of a thin cartridge that allows for the use of various culture substrates, ranging from conventional microporous polymeric membranes to 3D scaffolds/complex surfaces or organotypic tissues. The cartridge is inserted in a so-called "culture module", conceptualized as a multiwell-insert-like culture device, designed to facilitate standard TW procedures, enabling robust co-culture protocols, while allowing simple and controlled retrieval of the biological sample without compromising morphological integrity. In the present study, we demonstrated the functionality of the TTOP culture module optimizing a model of intestinal

epithelial barrier with polarized Caco-2 cells,[24,25] and of vascular endothelial barrier with EAhy-926 cells,[26] cultured over a commercially available microporous membrane inserted in the TTOP cartridge. We evaluated the barrier function of these models in physiological conditions and under inflammatory stimulation (with Tumor Necrosis Factor-α, TNF-α[27]). Finally, we coupled the gut and the vascular barrier models in TTOP, toward the in vitro mimicking of the GVB.

2. Results

2.1. Design for Rapid and Scalable Prototyping

The core of TTOP is a cartridge allowing to host either microporous polymeric membranes or 3D structures, as planar scaffolds (e.g., electrospun materials), where cells or organotypic tissues can be settled, or 3D organotypic models (**Figure 1a**). The cartridge is inserted in a culture module (Figure 1b), that presents multiple advantages: i) direct access to the biological sample; ii) easy recovery of the biological sample inside the cartridge, without morphological damages, for further accurate analyses; iii) the possibility to reposition in other compatible modules the cartridge including the biological sample and apply sequential treatments (e.g., bicompartmental perfusion).

The multilayer structure of the device is created through CO_2-laser micro-machining of 500-µm thick polymethylmethacrylate (PMMA) sheets, along with 100-µm thick acrylic double-sided pressure-sensitive adhesives (PSA) and 75-µm-thick hydrophobic tapes. This technique allows for a simple, low-cost, and rapid fabrication of devices (100 devices/procedure-5 hours, Figure S1, Supporting Information), providing good reproducibility.[28–30] The possibility to tune the culture area geometry and dimensions (Figure S2, Supporting Information) allowed us to obtain a standard 96-well plate's unit culture area (6.5-mm-diameter) obtained by cutting in the device center a circular window passing through all the layers. A microporous, track-etched polycarbonate (PC) membrane, hosted in the cartridge, served as a standard support to culture cell monolayers in a bicompartmental configuration. In this configuration, the overall dimensions of the TTOP were 19 × 19 mm, guaranteeing full compatibility with commercially available 12-well plates. A 380-µm thick sealing PSA is positioned forming a frame all around the cartridge. When the hydrophobic layers of the cartridge come in close contact with the hydrophobic layers of the culture module (consisting of an inferior and a superior pocket, Figure 1b), a hydrophobic sealing is generated, preventing fluid leakage between compartments (the pocket-cartridge system). This arrangement efficiently seals the cartridge in a sandwich-like fashion within the device.

Significantly, this technological solution, coupled with a straightforward snap-crack procedure facilitated by purposefully designed weakening carvings (Figure 1b) allows the extraction of the cartridge without causing any damage to the biological sample (Figure 1c; Figure S3, Supporting Information). The biological sample housed in the extracted cartridge can be stained and submitted to microscopy analyses using standard protocols. This avoids the need of a scalpel blade or punching for sample recovering, thus decreasing the risk of sample loss typical of the TW insert.

2.2. Pocket-Cartridge System Sealing Principle

Ensuring the maintenance of compartment separation is crucial in the study of barrier functions, as the regulation of inter-compartment molecular transfer should rely only on the functionality of the interposed cultured tissue. To assess the sealing durability of the pocket-cartridge system (Figure 1b), we devised two tests. First, we employed the Young–Laplace equation to model the pocket-cartridge interaction (Equation S1, Supporting Information), determining the minimum pressure required to break the hydrophobic valve (burst pressure, ΔP_{burst}, **Figure 2a**). This calculation considered a system with constant temperature and an equilibrium configuration between external pressure and surface tension ($\gamma_{L,V}$), and a distance (δ) between the pocket-cartridge hydrophobic layers ranging from 1 to 5 µm, comparable with the flatness tolerance. The functionality of the pocket-cartridge system was evaluated estimating the burst pressure in water and in complete culture medium (Dulbecco's Modified Eagle's Medium (DMEM) low-glucose, supplemented with 10% Foetal Bovine Serum (FBS) acting as a surfactant potentially altering the burst pressure). For this purpose, 30 TTOP culture modules were modified to include a barbed fluidic connector connecting the device to a syringe pump. Pressure values corresponding to fluid flow through the pocket and cartridge interface were evaluated inserting impermeable membranes within the culture modules to prevent fluid flow through the membrane itself (Figure 2b). Results from both water (n = 14) and FBS-enriched medium (n = 16) demonstrated that high-pressure values (188.10 ± 66.80 and 158.20 ± 68.82 mmHg) were required to break the hydrophobic valve. It is important to note that these high-pressure scenarios are unlikely to be encountered in a typical experimental workflow, where pressure values can range from 0 to 2 mmHg (considering a safety margin, the threshold for considering the device suitable for experiments was set at 10 mmHg, 5 times higher than the max pressure (Figure 2c,d). Subsequently, a second test was performed to assess the long-term functional stability of the pocket-cartridge system under working conditions. Specifically, TTOP culture modules with impermeable membranes were assembled, placed inside 12-well plates filled with complete culture medium, and hosted in a standard incubator for cell culture (37 °C and 5% CO_2). We evaluated the burst pressures (n > 5 for each time point) at 1, 2, 3, and 4 weeks (Figure 2e). Interestingly, the mean burst pressure decreased over time, probably due to a partial infiltration of FBS-enriched culture medium, but remaining highly above the threshold set as a working condition (week 1: ΔP_{burst} = 70.62 ± 28.99; week 2: 67.07 ± 37.7; week 3: 84.72 ± 68.54; week 4: 72.21 ± 39.88 mmHg, Figure 2f). We concluded that the system may withstand operational conditions, effectively preventing leakages, leaving the regulation of communication between compartments depending solely on the interposed biological sample.

2.3. Trans Epithelial/Endothelial Electrical Resistance Measurements in TTOP

In the study of tissue barriers, an essential consideration is the quantitative assessment of the barrier tightness. Trans

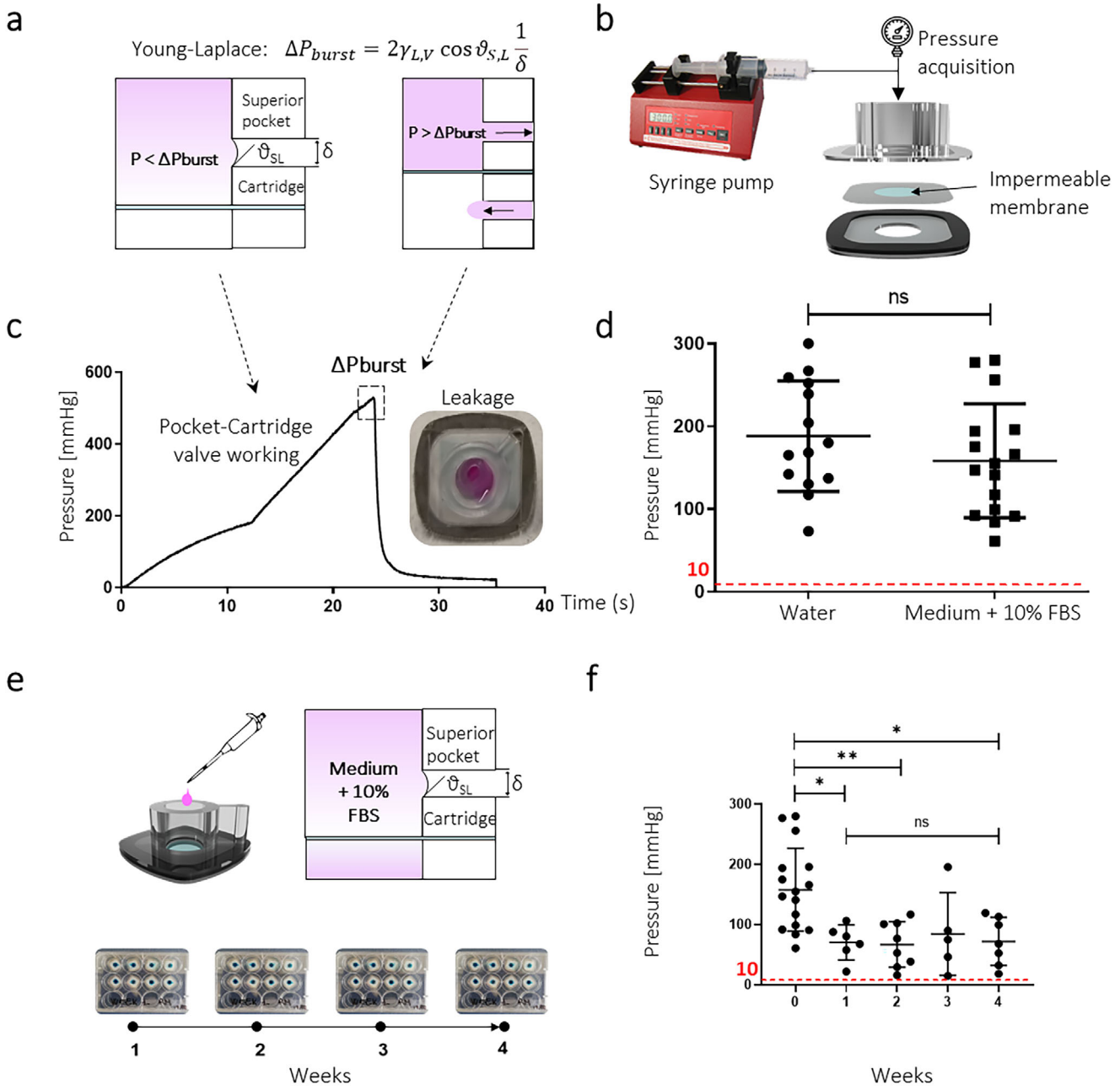

Figure 2. Pocket-Cartridge *hydrophobic valve* characterization. a) Pocket-cartridge schematic. Once in close contact, the hydrophobic layers of the cartridge and the inferior and superior pockets generate a strong *hydrophobic valve*, characterized by a contact angle at the liquid–solid interface $\vartheta_{S,L}$. Applying the Young–Laplace equation (Experimental Section, Supporting Information), it is possible to estimate the pressure needed to break the valve and let the liquid flow through the hydrophobic layers (ΔP_{burst} = burst pressure). b) Burst pressure measurement setup. Culture modules with impermeable membranes were connected to a syringe pump; a pressure sensor, positioned in derivation, acquired the pressure values in the device after the pump activation. c) Burst pressure assessment. Representative burst pressure curve where, upon reaching the burst pressure peak, the hydrophobic valve collapses, allowing fluid to flow from the apical to the basal compartment. d) Burst pressure values gathered using either water or FBS-enriched medium (water: $n = 14$, FBS-enriched medium: $n = 16$, unpaired t-test, $p = 0.24$). The red dotted line represents a designated threshold below which compartmental sealing is considered unreliable. e) Long-term functional stability of the pocket-cartridge system. Burst pressure evaluation procedure assessing burst pressure values every week for 4 weeks under continuous working conditions. f) Burst pressure values showing burst pressure decreasing after 1 week, then remaining stable in the next weeks, always above the designated threshold (Tukey's multiple comparisons test was used; p-value < 0.05 is considered significant and shown as *; $p < 0.01$ is indicated by **).

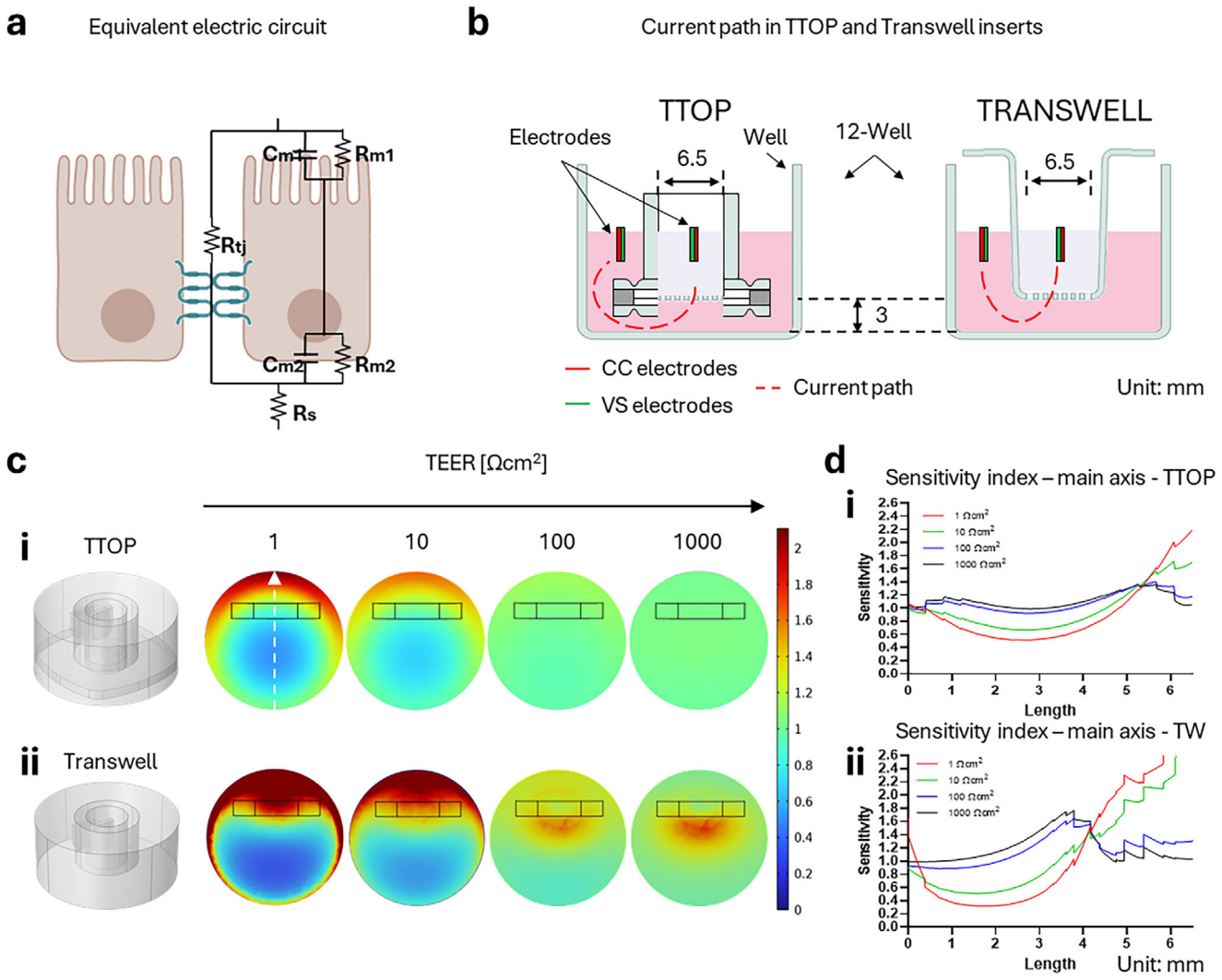

Figure 3. TEER in TTOP culture module and *TW* insert. a) Equivalent electric circuit for an epithelial cellular layer. In TEER measurements, membrane capacitances act as open circuits (R_m, C_m), allowing to measure the paracellular resistance R_{tj} representing the selective ion route through cell tight junctions and the solution resistance (R_s). b) Schematic representation of chopstick-like electrodes (red side = Current Carrying (CC); green side = Voltage Sensing (VS)) for use with TTOP culture module and standard *TW* insert. To measure TEER one chopstick electrode is inserted in the apical compartment and another one in the basolateral compartment. The red-dotted line sketches the current path in the two systems, for qualitative comparison. c) 2D normalized planar sensitivity distributions along the cell barrier surface (rainbow color map) in the *x*–*y* plane for TTOP culture module (i) and TW insert (ii) and d) sensitivity distribution along the cell barrier through the axis (white-dotted arrow shown in the 2D sensitivity map in TTOP device at TEER = 1) for TTOP culture module (i) and TW insert (ii). Results are presented for different TEER values (1-10-100-1000 Ωcm2), length unit in mm.

Epithelial/Endothelial Electrical Resistance (TEER), a cumulative measurement of two ion-conductive pathways – the paracellular resistance and the transcellular resistance (**Figure 3**a) – has gained widespread recognition as a minimally invasive, real-time, label-free technique for in vitro applications. However, the TEER measurements can be influenced by various factors, including electrode positioning, tilting angle, and electric current path within the system. Notably, when measuring the TEER of a cell culture, the precise location of the electrodes combined to the geometry of the support may lead to local differences in the measured resistance. According to Grimnes and Martinsen, a sensitivity factor (S) can be defined to represent the influence of each zone on the total measured value.[31] Ideally, the S should approach 1 across the whole sample, ensuring a TEER value that accurately reflects the barrier behavior. To address these issues, we developed a finite element method (FEM) model using the AC/DC module from the commercial software COMSOL Multiphysics v.6.0 to map the distribution of S over the cultured area, comparing the TTOP culture insert and TW insert (serving as standard control) in the numerical study.[32,33] A constant current was applied through the current-carrying electrodes (CC electrodes, Figure 3b). To calculate S, an additional simulation was conducted by interchanging voltage sensing electrodes (VS electrodes) and CC electrodes, that is, applying current through the previous VS electrodes and recording voltage through the previous CC electrodes. A parametric sweep of TEER values (1, 10, 100, and 1000 Ω cm^2) spanning the range reported in the literature for epithelial or endothelial barriers,[34–37] was simulated.

As expected, in both TTOP and TW insert, the regions near the electrodes exert a larger impact on TEER than those situated farther away, and sensitivity uniformity improves with increasing TEER. This accounts for minor TEER variations attributed to the non-reproducible placement of the manually positioned chopstick electrodes. Interestingly, the sensitivity distribution in the TTOP culture module demonstrated greater homogeneity over the area compared to the TW inserts (Figure 3ci,ii). Considering the center of the device ($x = 3.25$ mm; $y = 3.25$ mm), we compared S of TTOP and TW insert at TEER values of 100 and 1000 Ω cm^2, which are typical normalized values. We observed *S*-values closer to 1 in the TTOP culture module (TEER 100: 0.96; TEER 1000: 1) in comparison to the TW insert (TEER 100: 1.43; TEER 1000: 1.58) (Figure 3di,ii). This phenomenon can be attributed to the current path from one electrode to the other. The TTOP geometry involves a longer current path, increasing the equivalent solution resistance on one side and concurrently reducing the heterogeneity of the distribution of S on the other. Nevertheless, given that the total measured resistance in TTOP is higher than that of TW inserts, this could impact on the measurement, particularly when TEER values fall within the range of 1–10 Ω cm^2. To address this concern in our experimental procedures, we incorporated at least two cell-free culture modules as blank controls and to further improve measurement repeatability, we employed a 3D-printed holed lid that ensured proper centering of the TEER electrodes (Figure S4, Supporting Information). Mean of the blank values was then subtracted from the measured value and the resulting value normalized by the cultured area.

The implementation of this process was intended to effectively mitigate the overall variability in the measurements, that often arises from the manual placement of electrodes and laboratory rapid prototyping fabrication processes.

2.4. Establishment of Caco-2 Cell Culture as an Intestinal Epithelial Model in TTOP

To establish the system functionality, a Caco-2 epithelial cell in vitro model of the intestinal epithelial barrier[24,25] was optimized in TTOP. Cells settled over laminin-coated PC membranes within TTOP and on laminin-coated TW inserts (serving as gold standard control) were cultured to obtain monolayers (**Figure 4a**). Uncoated TTOP devices were included as controls to confirm the effect of laminin coating (Figure S6, Supporting Information). The laminin-based coating promotes cell adhesion and mitigates variability due to differences in PC membranes hosted in the two systems.[3] We investigated the suitability of both systems to measure TEER during the culture period (measurements performed every 3 days) and to perform microscopy. Interestingly, TEER values over time were comparable between TTOP and TW systems for Caco-2 cells cultured on laminin-coated membranes. In both systems, TEER values ≥400 Ω cm^2 were reached within 14 days (Figure 4b).[38] In fact, since TEER values are associated with a well-developed tight junction network,[9,24] which is a hallmark of Caco-2 polarization and epithelial barrier establishment, these results suggest that both systems support comparable epithelial barrier formation. Confocal microscopy analysis of nuclei and ZO-1 staining in Caco-2 monolayers cultured for 14 days on laminin-coated PC membranes showed a comparable and diffuse pattern in both TTOP and TW systems, confirming the formation of tight and polarized epithelial layers in both systems (Figure 4c).[39] As expected, uncoated TTOP devices exhibited slower TEER development compared to laminin-coated devices (Figure S6a, Supporting Information) as well as a less organized ZO-1 network (Figure S6b,c, Supporting Information). To test the responsivity of the barrier toward inflammatory stimuli, we treated Caco-2 cells with TNF-α (Figure 4d), a pro-inflammatory cytokine well known for inducing leaks in the intestinal epithelial barrier, increasing permeability.[35,40,41] After 48 h of stimulation with TNF-α (added into the apical compartment) of Caco-2 cell samples in TTOP, a significant decrease in the electrical resistance versus untreated samples was measured ($p = 0.0001$, Figure 4e). To verify the change in barrier permeability induced by TNF-α, the LY assay was performed.[40] In agreement with TEER data,[39] the analysis of the amount of LY crossing the barrier and accumulating into the basolateral compartment demonstrated higher levels of LY in the TNF-α treated versus untreated samples ($p < 0.0001$, Figure 4f). The effect of TNF-α treatment on cell tight junctions was analyzed by confocal microscopy, revealing a local decrease in ZO-1 fluorescence signal in TNF-α treated samples (Figure 4g; Figure S6e, Supporting Information). These data suggest that the increase of monolayer permeability found in TNF-α treated Caco-2 cells could be due to a reduction of tight junction complexes. In addition, the pro-inflammatory effect of the treatment with TNF-α was assessed by evaluating NOD-like receptor protein 3 (NLRP3) inflammasome pathway markers' mRNA expression (Interleukin 1β (IL-1β), NLRP3, and Nuclear Factor Kappa-light-chain-enhancer of activated B cells (NF-κB)) and the cytoplasm-to-nucleus translocation of the activated isoform of NF-κB (NF-κB p65 subunit). Although TNF-α stimulation did not increase the in Caco-2 monolayers cultured in TTOP (Figure S6f, Supporting Information), we observed a nuclear translocation of phosphorylated NF-κB in TNF-α treated samples (Figure S6g, Supporting Information), that could indicate post-transcriptional activation of the pathway, leading to the initiation of an inflammatory response.[42,43] These findings demonstrate the suitability of the TTOP device for functional characterization of tissue barriers. Notably, the modular design allows straightforward retrieval of the cultured samples, thereby facilitating downstream analyses such as gene expression profiling and in situ antibody staining, while minimizing disruption of sample integrity.

2.5. Establishment of EAhy-926 Vascular Endothelial Cell Model in TTOP

An approach similar to that for Caco-2 was applied to EAhy-926 hybridoma cell line (derived from human umbilical vein endothelium and A549/8 lung cancer cells), a recognized model of the endothelial barrier (**Figure 5a,d**).[26] EAhy-926 cells were cultured laminin-coated PC membrane within TTOP, and in laminin-coated TW insert for comparison (Figure 5a). Uncoated TTOP devices were included as controls to confirm the effect of laminin coating (Figure S7, Supporting Information). Despite EAhy-926 cells are not known for forming strict tight junctions,[44–46] we were able to monitor their growth rate

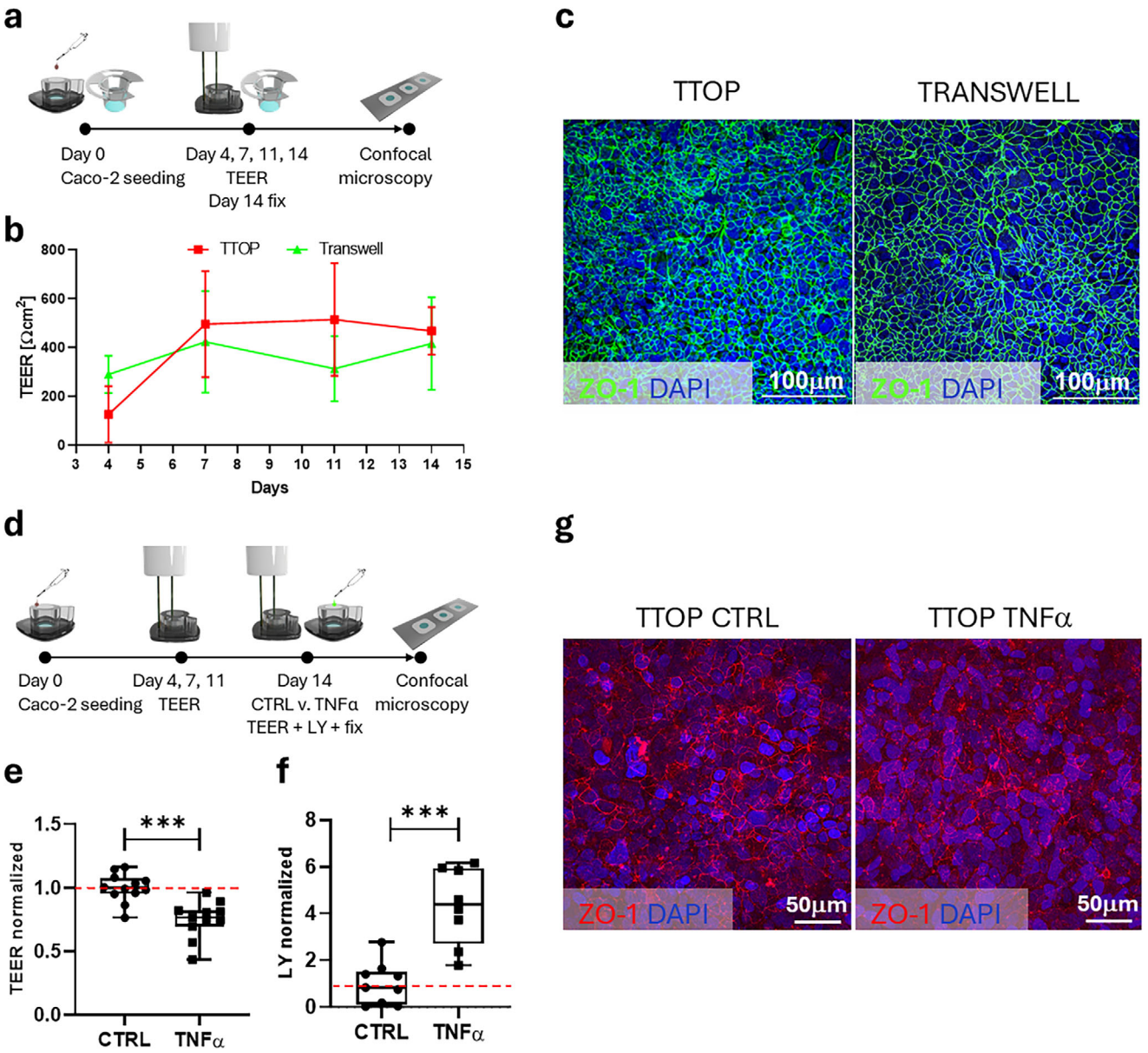

Figure 4. a) Experimental protocol for TTOP versus TW Caco-2 cultures. b) TEER measurements of Caco-2 cells during the cell monolayer formation in laminin-coated TTOP and laminin-coated TW insert. c) Representative confocal microscopy 2D extended focus images from 30× objective magnification are shown for TTOP and TW. Cells were stained for tight junction ZO-1 protein (ZO-1, green) and nuclei (DAPI, blue). d) Experimental protocol for TTOP versus TW Caco-2 permeability study after TNF-α treatment. e) Normalized fold-changes in TEER measurement and f) in permeability by LY assay in untreated (CTRL) versus TNF-α treated Caco-2 cells. Values are presented as boxes (min to max), dots indicate sample mean values. Unpaired t test is applied since data are normality distributions; p-value < 0.05 is considered significant; $p < 0.05$ is indicated by *, and $p < 0.01$ by **; $p < 0.001$ is indicated by ***. The red dotted line represents the normalized average of CTRLs. Raw values are shown in Figure S6h (Supporting Information). g) Representative confocal microscopy 2D extended focus images of Caco-2 cells with/without TNF-α treatment are shown. Cells were stained for ZO-1 (red) and nuclei with DAPI (blue). The 60× objective magnification are shown.

overtime (Figure 5b; Figure S7a, Supporting Information). TEER reached similar values at the end of the experiment, suggesting that comparable barriers were formed. Confocal microscopy showed well-developed, confluent monolayers by expression of the endothelial lineage marker Platelet Endothelial Cell Adhesion Molecule-1 (CD31/PECAM1)[47] (Figure 5c; Figure S7b,c, Supporting Information), thus confirming the establishment of endothelial barriers. TEER measured after stimulation demonstrated a significant reduction in the TNF-α-treated samples versus untreated ($p = 0.0159$, Figure 5e). Accordingly, the measure of permeability by Lucifer Yellow (LY) showed a significant accumulation of LY into the basolateral compartment in TNF-α treated samples versus untreated ($p < 0.0001$, Figure 5f). Confocal microscopy analysis of samples stained for filament- actin (F-actin) (by Phalloidin-tetramethylrhodamine (TRITC)) displayed a reorganization of the F-actin cytoskeleton (i.e., presence of peripheral

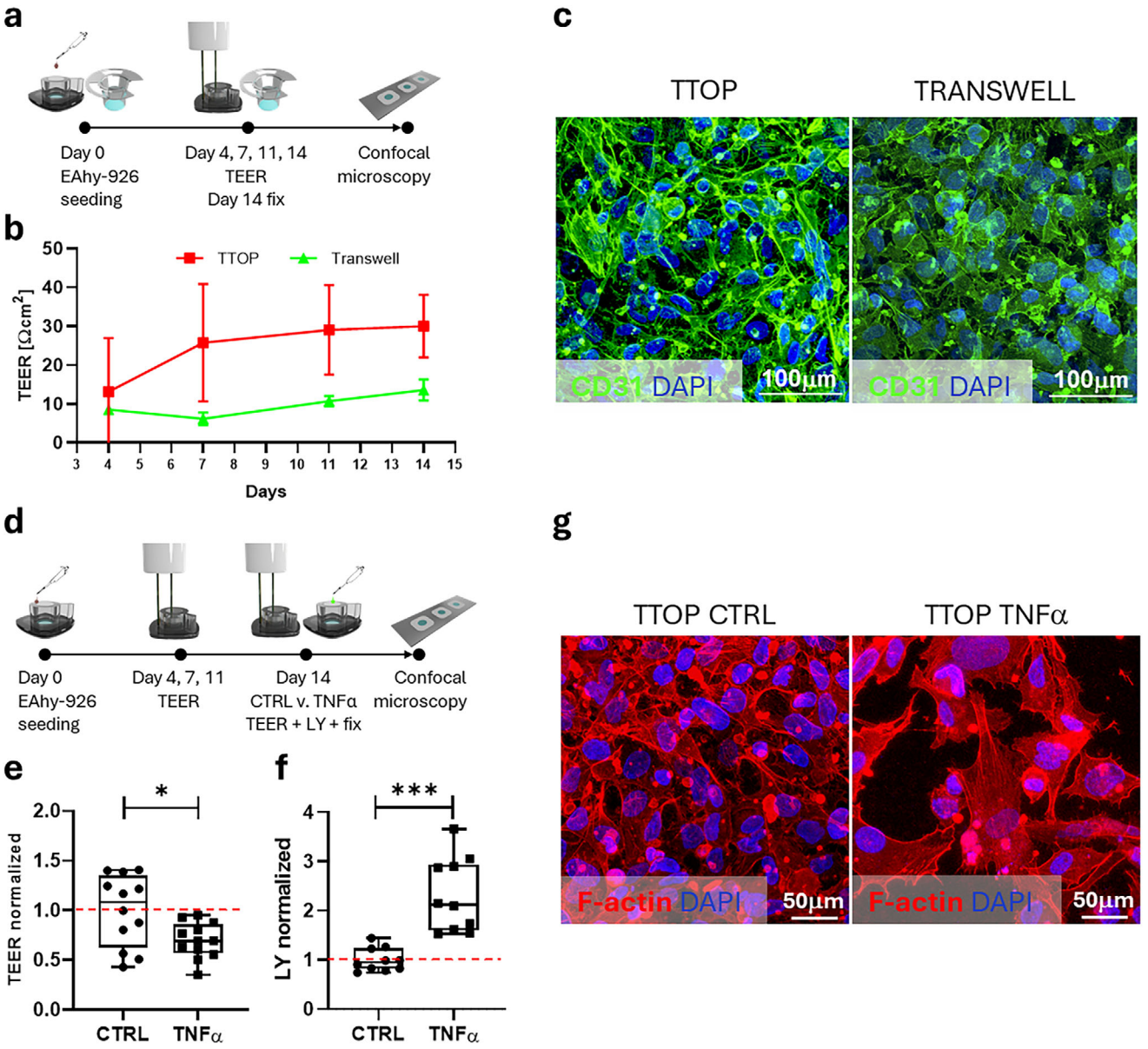

Figure 5. a) Experimental protocol for TTOP versus TW EAhy-926 cultures. b) TEER measurements of EAhy-926 endothelial cells during the cell monolayer formation in laminin-coated TTOP and laminin-coated TW insert. c) Representative confocal microscopy 2D extended focus images from 30× objective magnification are shown. Cells were stained for CD31/PECAM1 (CD31, green) and nuclei (DAPI, blue). d) Experimental protocol for TTOP versus TW EAhy-926 permeability study after TNF-α treatment. e) Normalized fold changes in TEER measurements and f) in permeability by LY in untreated (CTRL) versus TNF-α treated EAhy-926 cells. Values are presented as boxes and dots indicate sample mean values. Unpaired t-test is applied since data are normality distributions; p-value < 0.05 is considered significant and shown as *; $p < 0.01$ is indicated by **; $p < 0.001$ is indicated by ***. The red dotted line represents the normalized average of CTRLs. Raw values are shown in Figure S7h (Supporting Information). g) Representative confocal microscopy 2D extended focus images from 60× objective magnification of EAhy-926 cells with/without TNF-α treatment are shown. Changes in cytoskeleton structure were shown by labeling for Phallodin-TRITC (F-actin, red); nuclei were counterstained with DAPI (blue).

reinforced fibers and stress fibers in Figure 5g,) in TNF-α treated samples.[48] In addition, TNF-α treatment led to a significant decrease in cell density (Figure S7d, Supporting Information), accompanied by a reduction and redistribution of Vascula Endothelial -cadherin (VE-cad)[49] (Figure S7f, Supporting Information). and paralleled by a remarkable alteration in CD31/PECAM1 pattern (Figure S7g, Supporting Information). These observations indicate phenotypical changes and cytoskeleton alterations compatible with a loss of endothelial barrier integrity. Gene expression analysis by Real Time quantitative Polymerase chain reaction (RT-qPCR) revealed that TNF-α induced a significant increase in IL-1β, NRLP-3, and NF-kB genes (Figure S7e, Supporting Information); these data may indicate the activation of the inflammasome.[50]

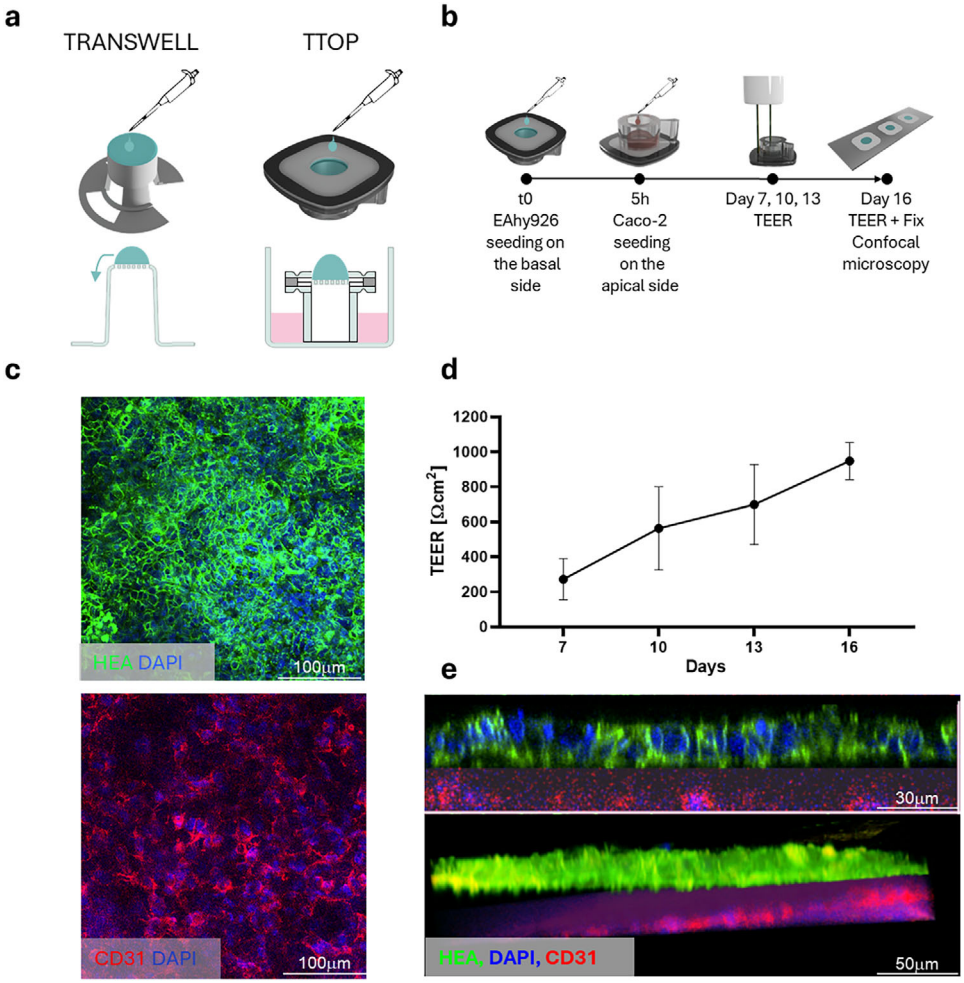

Figure 6. a) Schematics of TTOP and TW insert used in co-culture experiments. b) Experimental protocol for the seeding of Caco-2 and EAhy-926 on the opposite sides of the microporous membrane in TTOP. c) Representative confocal microscopy 2D extended focus images from 30× objective magnification are shown. Cells stained for HEA (green), CD31/PECAM1 (CD31, red), and nuclei (DAPI, blue) are shown. d) TEER measurements at 7, 10, 13, and 16 days during Caco-2 and EAhy-926 co-culture in laminin-coated TTOP are plotted. e) Representative cross-sectional images and 3D rendering confirmed the exclusive localization of Caco-2 and EAhy-926 cells on the opposite sides of the microporous membrane. Scale bars indicate magnification.

2.6. Co-Culture of Caco-2 and EAhy-926 Monolayers on TTOP: toward GVB Modeling

In the gut mucosa, the epithelial and endothelial barriers are adjacent and regulate the mucosal uptake of molecules and pathogens from the intestinal lumen and bloodstream, respectively. Taken together they constitute the GVB.[51] To build an in vitro model of the GVB, we combined the Caco-2 and EAhy-926 models, coculturing into TTOP the epithelial cells over the apical side of the coated membrane, and the endothelial cells over the basolateral side (**Figure 6**a,b). To assess the approach feasibility, we monitored the culture by TEER till reaching the value ≥ 400 Ω cm^2 (Figure 6d). Successive confocal microscope analysis of samples stained for HEA and CD31/PECAM1 confirmed the localization of HEA-stained Caco-2 cells on the upper side, and that of CD31/PECAM1 confined to EAhy-926 on the bottom side of membrane (Figure 6c,e). These preliminary data support the feasibility of TTOP for building biological barriers in both compartments, suggesting its usefulness to study GVB function and the endothelial–epithelial cross-talk.

3. Discussion

In the last decade, researchers and lately regulatory bodies[52] have spent many efforts to develop advanced lab culture platforms with the aim of recapitulating complex pathophysiological scenarios.[53] Several research groups[13–16,18,20,23,54–56] and companies (e.g., Altis Biosystems,[12,57] MatTek Inc.[10]) now offer primary human intestinal models in TW formats, enabling rapid and straightforward distribution for applications in biomedical and clinical research, while addressing key limitations associated with conventional Caco-2–based models.

Although most of these models have proven highly useful for studying intestinal barrier function, they still suffer from the intrinsic limitations of TW formats. These include: i) the restriction to microporous polymeric membranes as culture substrate,

which constrain direct physical contact between co-cultured cells and provide a rigid substrate poorly representative of the native intestinal ECM; ii) the complexity and poor reproducibility of co-culture procedures; and iii) the unreliable retrieval of biological samples, which often results in loss or damage of the specimen for end-point analyses. To meet the need for "easy-to-use" advanced devices compliant with standardized procedures, we developed TTOP, a novel bicompartmental cartridge-based platform. The modular design of TTOP allows to select and host a culture substrate of interest (e.g., porous membranes, 3D scaffolds, hydrogels) in a thin cartridge that can be placed in purposefully designed modules. The basic configuration of TTOP, hosting cell-culture-treated microporous membranes, allows single- or co-culture of various cell types in a bicompartmental setting, mimicking barrier tissues' microenvironmental conditions. At the end of the experiments, the cartridge can be retrieved without compromising the biological sample integrity,[58] allowing for the collection of reliable data. In fact, sample loss due to mishandling is a common limitation with conventional inserts often requiring scalpel cutting. Within the TTOP culture module, the retrieval can be performed on cartridges containing living cells, enabling to apply sequential treatments by moving the cartridge through different modules as needed. This "plug-and-play" modularity[60,61] can enable researchers to combine already set cell-culture protocols[7,8] with minimal adjustments, while leveraging the platform's modularity to achieve advanced and biologically relevant in vitro tissue models of physiological barriers.

As a starting point, we conceived, prototyped, and manufactured a bicompartmental culture module that enables the direct translation of conventional TW insert protocols for generating tissue barrier models.[9,62,63] The geometry of TTOP, allowing culture modules positioning within standard 12 well plates, enables its simple integration with standard laboratory tools[64] and assays (e.g., permeability,[65,66] oxygen gradient,[67] chemical gradient,[68] and TEER measurements),[59,69] unlike other microdevices that typically require customized solutions.[70–73]

When assessing barrier tissue functions, TEER is considered a standard assay utilized as a minimally invasive and quantitative method[69] for monitoring the establishment of tissue barriers overtime. Under this consideration, we first evaluate the suitability of our device for applying TEER measurements, by developing a FEM model[31–33] and comparing the performance of TTOP culture modules against TW inserts. The FEM model demonstrated that TTOP geometry allows a more homogenous contribution of the biological sample to the total resistance (as expressed by the sensitivity coefficient S) with respect to TW inserts (Figure 3c), hence guaranteeing a more representative evaluation of the tissue barrier tightness.

We cultured intestinal (Caco-2) and vascular (EAhy-926) monolayers on laminin coated microporous membranes,[3] to investigate the permeability of each monolayer. The laminin coating promoted the formation of a functional intestinal barrier, with TEER values rapidly increasing (Figure 4b) and comparable at day14 to those measured in other intestinal in vitro models at day 17–21.[65,74,75] Then, we applied a TNF-α treatment, mimicking an intestinal inflammatory stimulus, and we observed that Caco-2 permeability increased, as demonstrated by significant lowered TEER values and increased passage of LY in the basal compartment (Figure 4e,f; Figure S6e,h, Supporting Information). These findings are consistent with previous studies using Caco-2 cells monolayers[35,40,41] and suggest the suitability of the device for studying pathologic conditions.

On the other hand, EAhy-926 cells are known to establish a more permeable barrier, showing TEER values of about ten times less as compared to Caco-2.[44–46] However, in TNF-α treated samples of EAhy-926, we observed a significant decrease in TEER, accompanied by a reduction in cell density, indicating that leakage increase is paralleled by moderate rise in cell detachment (Figure 5e; Figure S7d,h, Supporting Information). Further evaluations of the intestinal and endothelial barriers confirmed permeability changes associated with barrier formation (via LY assay, Figures 4f,5f; Figures S6h,S7h, Supporting Information) and morphological alterations (observed through confocal microscopy, Figures 4c,5c; Figures S6g,S7f,g, Supporting Information). In these settings, the possibility to retrieve the sample without compromising its integrity offers a robust and precise tool for testing the expression of tight junctions and other markers, assessing their spatial distribution and potential alteration in cell monolayers.

Finally, we conducted a preliminary set of experiments demonstrating the suitability of TTOP for developing an in vitro model of the GVB, by combining intestinal and vascular monolayers on the opposite sides of the TTOP-coated membrane (Figure 6c,e). TTOP ability to co-culture cells on both sides of the culture substrate allows for easy flipping within the multi-well plate, enabling cells to be seeded and immediately placed in the incubator. Additionally, when flipped, the thickness of the PMMA layers provides walls to contain the medium with cells, preventing cell dispersion and ensuring a stable seeding configuration (Figure 6a; Figure S8, Supporting Information). In contrast, co-culturing cells in TW requires flipping the inserts outside from the multi-well plate and keeping the system under a biological cabinet until the cells attach, as the inserts do not fit the multi-well plate in the flipped position.[21,22] Some solutions have been proposed to address this issue, such as using a density-driven method to let cells float on the liquid meniscus and attach easily to the culture membrane[76] or using larger multi-well plate formats or Petri dishes to host the flipped insert. However, the introduction of a high-density liquid can alter the standard culture protocol and affect the experimental outcomes[77] and the use of other plates is often less stable, increasing the risk that the cell-containing droplet falls down from the membrane, resulting in uneven or failed seeding.

Despite the promising results, the GVB in TTOP should be further refined. In fact, both Caco-2 and EAhy-926 are immortalized cell lines and although immortalization guarantees rapid and standardized cultures, it also introduces a tumoral element that may affect cell responsivity, thus limiting their translational potential. Recent studies have demonstrated the potential of human-derived primary organoid models and, although these models are more expensive and complex to develop, they offer a more representative solution for mimicking intestinal physiology.[78–81] Notably, organoid monolayers have already been successfully cultured in TW inserts,[13,82] as shown by Stappenbeck and coworkers,[11,55,83] providing background protocols easily applicable into TTOP modules.

Another important factor to consider is the culture substrate, as recent studies have shown that its composition, stiffness, and

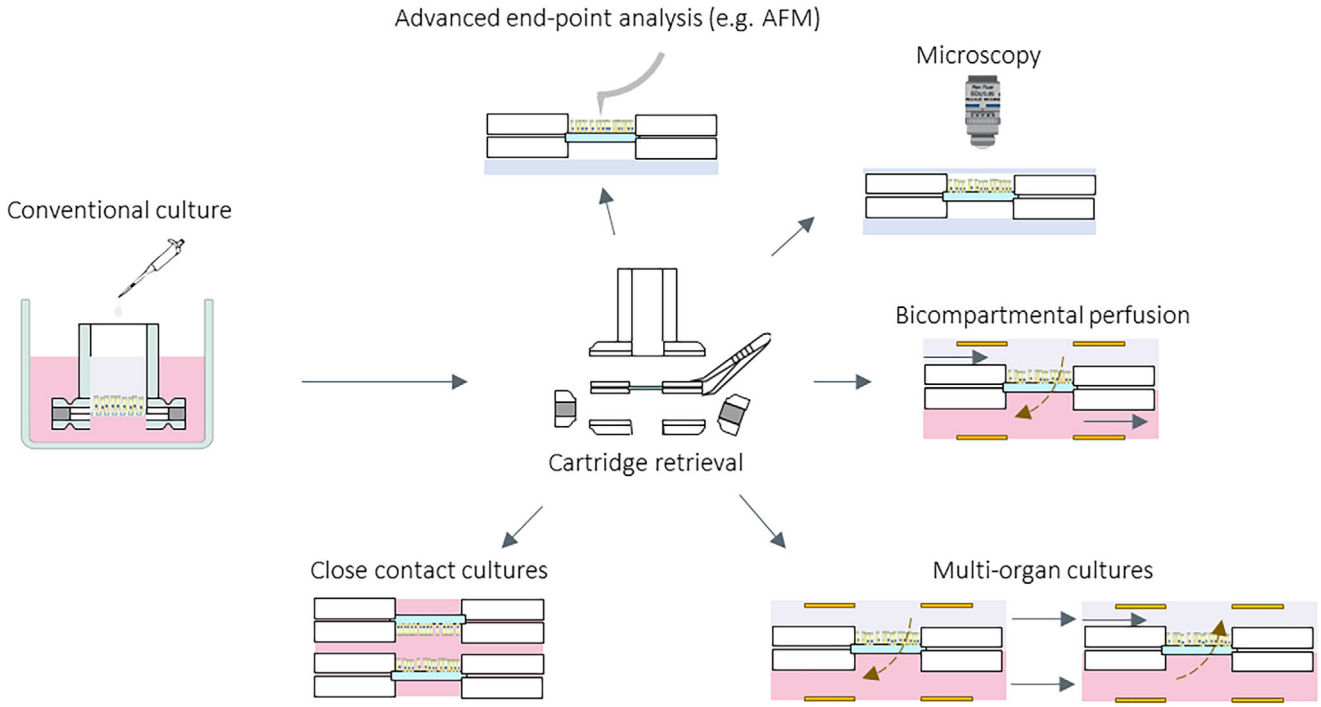

Figure 7. Schematics of TTOP cartridge retrieval and reuse. The controlled retrieval of the cartridge enables to carry out conventional and advanced end-point analysis, as well as the "plug-and-play" conversion from conventional static to more representative microenvironmental conditions (e.g., bicompartmental perfusion, combination of different cartridges in multi-organ dynamic cultures or close contact co-cultures, with TEER electrodes integrated).

3D structure critically impact cell behavior.[15,84,85] While this work utilized standard microporous polymeric membranes to achieve a direct comparison with conventional TW inserts, the versatility of the TTOP cartridge-based culture modules could be explored to accommodate 3D electrospun scaffolds,[86] pre-shaped hydrogels,[15,18,84] organotypic cultures,[10] and patient-derived tissue slices,[87] thus achieving an enhanced representation of the human extracellular microenvironment (Figure S9, Supporting Information).

TTOP has been designed as a modular platform. Here we focused on presenting the culture module of our platform, designed for the straightforward translation of conventional TW protocols under conventional static conditions. However, we recognize that incorporating apical and basal perfusion is crucial for sustaining cell differentiation and replicating key physiological cues, which are unattainable in static conditions.[58,88,89] In fact, over the past decade, microphysiological systems (MPS) and organ on chips have emerged as novel platforms to study intestinal-vascular function on in vitro models of health and disease.[90] These complex gut models enable the culture of cells, organoids, or ex vivo tissue explants under dynamic stimuli, highlighting the importance of incorporating key chemical, physical, and mechanical stimuli in vitro to generate more physiologically relevant and predictive models.[68,87,91–95] For example, apical and basal perfusion strongly promotes villi-like structure formation and tissue maturation, by altering the delivery or removal of soluble signaling factors as well as applying a direct fluid shear stress to the epithelial cells, as shown by Ingber and colleagues.[68,92] Moreover, these systems are commonly equipped with TEER sensors, enabling continuous and automated monitoring of barrier integrity throughout the culture period.[96] However, such systems are often difficult to translate from bioengineering to biological laboratories, hampering their broader adoption in biomedical and clinical research.[73] For this reasons, the possibility to retrieve living samples within the TTOP cartridge will be leveraged to demonstrate the "plug-and-play" conversion from conventional static to bicompartmental perfusion condition thus enabling complex studies on human patho-physiology (**Figure 7**). Therefore, we aim to create new modules that can provide a precise and controlled dynamic microenvironment, with integrated TEER electrodes, while maintaining simple, conventional processes that can be rapidly implemented in regulated settings, including pharmaceutical companies, Contract Research Organizations, and industry.[84,97,98] Taken together, these elements support our claim that TTOP has the potential to significantly impact biological and biomedical research by providing an easy to use, versatile and modular in vitro platform to the wide biomedical community.

4. Conclusion

We have developed TTOP, validating a modular, versatile, and user-friendly device consisting of a retrievable cartridge and a bicompartmental culture module, allowing for a seamless transition of procedures carried out with conventional culture inserts into more advanced study models. We have demonstrated that TTOP is well-suited for permeability assays and TEER measurements. Importantly, the cartridge easy removal allowed for

downstream characterization, including gene expression and in situ antibody staining with minimal disruption of the biological sample.

Our study exploited the basic potential of TTOP to setup and characterize in vitro models of the GVB in respect of refine, reduce, and replace (3R) policies.

Supporting Information

Supporting Information is available from the Wiley Online Library or from the author.

Acknowledgements

L.P.C. and M.L. contributed equally to this work. This work was funded by Proof of Concept Grant awarded by Poli360 Technology Transfer Fund and by the National Plan for NRRP Complementary Investments (PNC, established with the decree-law 6 May 2021, n. 59, converted by law n. 101 of 2021) in the call for the funding of research initiatives for technologies and innovative trajectories in the health and care sectors (Directorial Decree n. 931 of 06-06-2022) – project n. PNC0000003 – AdvaNced Technologies for Human-centerEd Medicine (project acronym: ANTHEM). This work reflects only the authors' views and opinions, neither the Ministry for University and Research nor the European Commission can be considered responsible for them. The authors thank the ALEMBIC Facility, and advanced microscopy laboratory established by the IRCCS San Raffaele Hospital and the Vita-Salute San Raffaele University, for providing access to confocal microscopes.

Conflict of Interest

Since March 2022, L.P.C., M.L., C.F., G.B.F., and M.S. are cofounders of TTOP Srl and hold an equity interest in the company. TTOP is developing cartridge-based technologies including the culture modules and cartridges used in this study. L.P.C., M.L., C.F., G.B.F., and M.S. are inventors on a granted Italian patent now under PCT extension (WO2022043815A1) related to the technology. The other authors declare no competing financial interest.

Data Availability Statement

The data that support the findings of this study are available on request from the corresponding author. The data are not publicly available due to privacy or ethical restrictions.

Keywords

advanced in vitro systems, gut–vascular barrier (GVB), inflammatory stimuli, microphysiological systems (MPS), modularity, retrievable cartridge, trans epithelial electrical resistance (TEER)

Received: January 10, 2025
Revised: August 26, 2025
Published online:

[1] Y. B. Arık, M. W. van der Helm, M. Odijk, L. I. Segerink, R. Passier, A. van den Berg, A. D. van der Meer, *Biomicrofluidics* **2018**, *12*, 042218.
[2] I. Spadoni, E. Zagato, A. Bertocchi, R. Paolinelli, E. Hot, A. Di Sabatino, F. Caprioli, L. Bottiglieri, A. Oldani, G. Viale, G. Penna, E. Dejana, M. Rescigno, *Science* **2015**, *350*, 830.
[3] M. D. Basson, G. Turowski, N. J. Emenaker, *Exp. Cell Res.* **1996**, *225*, 301.
[4] P. Brescia, M. Rescigno, *Trends Mol. Med.* **2021**, *27*, 844.
[5] F. Araújo, B. Sarmento, *Int. J. Pharm.* **2013**, *458*, 128.
[6] I. J. Hidalgo, T. J. Raub, R. T. Borchardt, *Gastroenterology* **1989**, *96*, 736.
[7] P. Artursson, J. Karlsson, *Biochem. Biophys. Res. Commun.* **1991**, *175*, 880.
[8] P. Artursson, K. Palm, K. Luthman, *Adv. Drug Delivery Rev.* **2012**, *64*, 280.
[9] I. Hubatsch, E. G. E. Ragnarsson, P. Artursson, *Nat. Protoc.* **2007**, *2*, 2111.
[10] S. Ayehunie, T. Landry, Z. Stevens, A. Armento, P. Hayden, M. Klausner, *Pharm. Res.* **2018**, *35*, 72.
[11] K. L. VanDussen, J. M. Marinshaw, N. Shaikh, H. Miyoshi, C. Moon, P. I. Tarr, M. A. Ciorba, T. S. Stappenbeck, *Gut* **2015**, *64*, 911.
[12] Y. Wang, C. E. Sims, N. L. Allbritton, *Anal. Chem.* **2022**, *94*, 9345.
[13] C. W. Wright, N. Li, L. Shaffer, A. Hill, N. Boyer, S. E. Alves, S. Venkataraman, K. Biswas, L. A. Lieberman, S. Mohammadi, *Sci. Rep.* **2023**, *13*, 16357.
[14] N. J. Darling, C. L. Mobbs, A. L. González-Hau, M. Freer, S. Przyborski, *Front. Bioeng. Biotechnol.* **2020**, *8*.
[15] N. Torras, J. Zabalo, E. Abril, A. Carré, M. García-Díaz, E. Martínez, *Biomater. Adv.* **2023**, *153*, 213534.
[16] M. B. Paul, M. Schlief, H. Daher, A. Braeuning, H. Sieg, L. Böhmert, *Vitr. Model.* **2023**, *2*, 43.
[17] J. F. Staab, J. M. Lemme-Dumit, R. Latanich, M. F. Pasetti, N. C. Zachos, *Curr. Protoc. Immunol.* **2020**, *131*, 113.
[18] S. S. Hinman, A. Massaro, Y. Wang, C. E. Sims, R. Kim, N. L. Allbritton, *Adv. Biol.* **2022**, *6*, 2200129.
[19] M. Kasendra, R. Luc, J. Yin, D. V. Manatakis, G. Kulkarni, C. Lucchesi, J. Sliz, A. Apostolou, L. Sunuwar, J. Obrigewitch, K.-J. Jang, G. A. Hamilton, M. Donowitz, K. Karalis, *Elife* **2020**, *9*, 50135.
[20] S. Zeiringer, L. Wiltschko, C. Glader, M. Reiser, M. Absenger-Novak, E. Fröhlich, E. Roblegg, *Mol. Pharmaceutics* **2023**, *20*, 5173.
[21] Y. Lu, J. Ma, G. Lin, *Food Chem. Toxicol.* **2019**, *129*, 391.
[22] V. Zaderer, M. Hermann, C. Lass-Flörl, W. Posch, D. Wilflingseder, *Cells* **2019**, *8*, 1292.
[23] J. M. Lemme-Dumit, M. Doucet, N. C. Zachos, M. F. Pasetti, *MBio* **2022**, *13*, 00944.
[24] Y. Sambuy, I. De Angelis, G. Ranaldi, M. L. Scarino, A. Stammati, F. Zucco, *Cell Biol. Toxicol.* **2005**, *21*, 1.
[25] I. De Angelis, L. Turco, *Curr. Protoc. Toxicol.* **2011**, *47*, 20.6.1.
[26] Z. J. Lu, Y. Q. Ren, G. P. Wang, Q. Song, M. Li, S. S. Jiang, T. Ning, Y. S. Guan, J. L. Yang, F. Luo, *J. Exp. Clin. Cancer Res.* **2009**, *28*, 16.
[27] S. H. Lee, *Intest. Res.* **2015**, *13*, 11.
[28] C. Matellan, A. E. Del Río Hernández, *Sci. Rep.* **2018**, *8*, 6971.
[29] H. Li, Y. Fan, R. Kodzius, I. G. Foulds, *Microsyst. Technol.* **2012**, *18*, 373.
[30] X. Chen, T. Li, Q. I. Gao, *Surf. Rev. Lett.* **2019**, *26*.
[31] S. Grimnes, Ø. G. Martinsen, *J. Phys. D: Appl. Phys.* **2007**, *40*, 9.
[32] J. Yeste, X. Illa, C. Gutiérrez, M. Solé, A. Guimerà, R. Villa, *J. Phys. D. Appl. Phys.* **2016**, *49*, 375401.
[33] L. Cacopardo, J. Costa, S. Giusti, L. Buoncompagni, S. Meucci, A. Corti, G. Mattei, A. Ahluwalia, *Biosens. Bioelectron.* **2019**, *140*, 111340.
[34] A. Béduneau, C. Tempesta, S. Fimbel, Y. Pellequer, V. Jannin, F. Demarne, A. Lamprecht, *Eur. J. Pharm. Biopharm.* **2014**, *87*, 290.
[35] L. M. Feighery, S. W. Cochrane, T. Quinn, A. W. Baird, D. O'Toole, S.-E. Owens, D. O'Donoghue, R. J. Mrsny, D. J. Brayden, *Pharm. Res.* **2008**, *25*, 1377.

[36] C. Hilgendorf, H. Spahn-Langguth, C. G. Regårdh, E. Lipka, G. L. Amidon, P. Langguth, *J. Pharm. Sci.* **2000**, *89*, 63.
[37] M. Amini, J. Hisdal, H. Kalvøy, *J. Electr. Bioimpedance* **2018**, *9*, 142.
[38] T. Y. Ma, G. K. Iwamoto, N. T. Hoa, V. Akotia, A. Pedram, M. A. Boivin, H. M. Said, *Am. J. Physiol. Liver Physiol.* **2004**, *286*, G367.
[39] M. A. Odenwald, W. Choi, W. T. Kuo, G. Singh, A. Sailer, Y. Wang, L. Shen, A. S. Fanning, J. R. Turner, *J. Biol. Chem.* **2018**, *293*, 17317.
[40] C. L. Pires, C. Praça, P. A. T. Martins, A. L. M. Batista de Carvalho, L. Ferreira, M. P. M. Marques, M. J. Moreno, *Pharmaceutics* **2021**, *13*, 1563.
[41] B. Srinivasan, A. R. Kolli, M. B. Esch, H. E. Abaci, M. L. Shuler, J. J. Hickman, *SLAS Technol.* **2015**, *20*, 107.
[42] T. Riedlinger, R. Liefke, J. Meier-Soelch, L. Jurida, A. Nist, T. Stiewe, M. Kracht, M. L. Schmitz, *FASEB J.* **2019**, *33*, 4188.
[43] S. Giridharan, M. Srinivasan, *J. Inflamm. Res.* **2018**, *11*, 407.
[44] F. Wei, S. Liu, L. Luo, N. Gu, Y. Zeng, X. Chen, S. Xu, D. Zhang, *Int. Immunopharmacol.* **2017**, *46*, 220.
[45] Y. Wang, A. Adamcakova-Dodd, B. R. Steines, X. Jing, A. K. Salem, P. S. Thorne, *NanoImpact* **2020**, *18*, 100215.
[46] A. Suttitheptumrong, N. Rawarak, O. Reamtong, K. Boonnak, S. Pattanakitsakul, *Proteomics* **2018**, *18*, 1800215.
[47] L. Piali, P. Hammel, C. Uherek, F. Bachmann, R. H. Gisler, D. Dunon, B. A. Imhof, *J. Cell Biol.* **1995**, *130*, 451.
[48] S. Y. Lee, *Int. J. Nanomed.* **2011**, *6*, 179.
[49] D. Vestweber, *Arterioscler. Thromb. Vasc. Biol.* **2008**, *28*, 223.
[50] G. E., Y. Cao, S. Bhattacharya, S. Dutta, E. Wang, D. Mukhopadhyay, *J. Biol. Chem.* **2012**, *287*, 3029.
[51] N. Di Tommaso, F. Santopaolo, A. Gasbarrini, F. R. Ponziani, *Int. J. Mol. Sci.* **2023**, *24*, 1470.
[52] E. Y. Adashi, D. P. O. M. Msls, I. G. C. Jd, *Am. J. Med.* **2023**, *136*, 853.
[53] J. Rogal, K. Schlünder, P. Loskill, *ACS Biomater. Sci. Eng.* **2022**, *8*, 4643.
[54] E. Floor, J. Su, M. Chatterjee, E. S. Kuipers, N. IJssennagger, F. Heidari, L. Giordano, R. W. Wubbolts, S. M. Mihaila, D. A. C. Stapels, Y. Vercoulen, K. Strijbis, *Gut Microbes* **2025**, *17*, 2434685.
[55] C. Günther, B. Winner, M. F. Neurath, T. S. Stappenbeck, *Gut* **2022**, *71*, 1892.
[56] J. Markus, T. Landry, Z. Stevens, H. Scott, P. Llanos, M. Debatis, A. Armento, M. Klausner, S. Ayehunie, *Vitr. Cell. Dev. Biol. – Anim.* **2021**, *57*, 160.
[57] C. M. Pike, B. Zwarycz, B. E. McQueen, M. Castillo, C. Barron, J. M. Morowitz, J. A. Levi, D. Phadke, M. Balik-Meisner, D. Mav, *bioRxiv* **2024**, *41*, 425.
[58] C. M. Leung, P. de Haan, K. Ronaldson-Bouchard, G.-A. Kim, J. Ko, H. S. Rho, Z. Chen, P. Habibovic, N. L. Jeon, S. Takayama, M. L. Shuler, G. Vunjak-Novakovic, O. Frey, E. Verpoorte, Y.-C. Toh, *Nat. Rev. Methods Prim.* **2022**, *2*, 33.
[59] W. Shang, C. Y. Chen, K. Lo, G. F. Payne, W. E. Bentley, *Sens. Actuators, B* **2019**, *295*, 30.
[60] Y. S. Zhang, J. Aleman, S. R. Shin, T. Kilic, D. Kim, S. A. Mousavi Shaegh, S. Massa, R. Riahi, S. Chae, N. Hu, H. Avci, W. Zhang, A. Silvestri, A. Sanati Nezhad, A. Manbohi, F. De Ferrari, A. Polini, G. Calzone, N. Shaikh, P. Alerasool, E. Budina, J. Kang, N. Bhise, J. Ribas, A. Pourmand, A. Skardal, T. Shupe, C. E. Bishop, M. R. Dokmeci, A. Atala, et al., *Proc. Natl. Acad. Sci. U. S. A.* **2017**, *114*, E2293.
[61] M. Ishahak, J. Hill, Q. Amin, L. Wubker, A. Hernandez, A. Mitrofanova, A. Sloan, A. Fornoni, A. Agarwal, *Front. Bioeng. Biotechnol.* **2020**, *8*.
[62] S. Youhanna, V. M. Lauschke, *J. Pharm. Sci.* **2021**, *110*, 50.
[63] H. Sun, E. C. Chow, S. Liu, Y. Du, K. S. Pang, *Expert Opin. Drug Metab. Toxicol.* **2008**, *4*, 395.
[64] M. Kus, I. Ibragimow, H. Piotrowska-Kempisty, *Pharmaceutics* **2023**, *15*, 2523.
[65] M. H. Macedo, A. S. Barros, E. Martínez, C. C. Barrias, B. Sarmento, *J. Controlled Release* **2022**, *341*, 414.
[66] T. S. Frost, L. Jiang, R. M. Lynch, Y. Zohar, *Micromachines* **2019**, *10*, 533.
[67] R. Kim, P. J. Attayek, Y. Wang, K. L. Furtado, R. Tamayo, C. E. Sims, N. L. Allbritton, *Biofabrication* **2020**, *12*, 015006.
[68] W. Shin, C. D. Hinojosa, D. E. Ingber, H. J. Kim, *iScience* **2019**, *15*, 391.
[69] B. Srinivasan, A. R. Kolli, M. B. Esch, H. E. Abaci, M. L. Shuler, J. J. Hickman, *J. Lab. Autom.* **2015**, *20*, 107.
[70] Q. Ramadan, M. Zourob, *Biomicrofluidics* **2020**, *14*, 041501.
[71] S. Halldorsson, E. Lucumi, R. Gómez-Sjöberg, R. M. T. Fleming, *Biosens. Bioelectron.* **2015**, *63*, 218.
[72] A. Nicolas, F. Schavemaker, K. Kosim, D. Kurek, M. Haarmans, M. Bulst, K. Lee, S. Wegner, T. Hankemeier, J. Joore, K. Domansky, H. L. Lanz, P. Vulto, S. J. Trietsch, *Lab Chip* **2021**, *21*, 1676.
[73] O. Y. F. Henry, R. Villenave, M. J. Cronce, W. D. Leineweber, M. A. Benz, D. E. Ingber, *Lab Chip* **2017**, *17*, 2264.
[74] J. Wang, C. Han, W. Ta, R. Liu, X. He, W. Lu, *J. Drug Delivery Sci. Technol.* **2021**, *62*, 102366.
[75] S. Lopez-Escalera, A. Wellejus, *Biochem. Biophys. Rep.* **2022**, *31*, 101314.
[76] H. Viola, K. Washington, C. Selva, J. Grunwell, R. Tirouvanziam, S. Takayama, *Adv. Healthcare Mater.* **2021**, *10*, 2100879.
[77] N. Ronda, F. Potì, A. Palmisano, R. Gatti, G. Orlandini, U. Maggiore, A. Cabassi, G. Regolisti, E. Fiaccadori, *Vascul. Pharmacol.* **2013**, *58*, 39.
[78] L. F. Lorenzo-Martín, N. Broguiere, J. Langer, L. Tillard, M. Nikolaev, G. Coukos, K. Homicsko, M. P. Lutolf, *Nat. Biotechnol.* **2024**, *43*, 727.
[79] M. J. Workman, J. P. Gleeson, E. J. Troisi, H. Q. Estrada, S. J. Kerns, C. D. Hinojosa, G. A. Hamilton, S. R. Targan, C. N. Svendsen, R. J. Barrett, *Cmgh* **2018**, *5*, 669.
[80] H. Yu, N. M. Hasan, J. G. In, M. K. Estes, O. Kovbasnjuk, N. C. Zachos, M. Donowitz, *Annu. Rev. Physiol.* **2017**, *79*, 291.
[81] T. Recaldin, B. Gjeta, L. Steinacher, M. F. Harter, L. Adam, M. Nikolaev, R. Krese, U. Kilik, D. Popovic, M. Almato-Bellavista, K. Kromer, M. Bscheider, L. Cabon, J. G. Camp, N. Gjorevski, *bioRxiv* **2023**, 2023.
[82] J. E. Speer, Y. Wang, J. K. Fallon, P. C. Smith, N. L. Allbritton, *J. Biol. Eng.* **2019**, *13*, 36.
[83] Y. Wang, I.-L. Chiang, T. E. Ohara, S. Fujii, J. Cheng, B. D. Muegge, A. Ver Heul, N. D. Han, Q. Lu, S. Xiong, F. Chen, C.-W. Lai, H. Janova, R. Wu, C. E. Whitehurst, K. L. VanDussen, T.-C. Liu, J. I. Gordon, L. D. Sibley, T. S. Stappenbeck, *Cell* **2019**, *179*, 1144.
[84] M. Hofer, M. A. Duque-correa, M. P. Lutolf, **2024**, bioRxiv, https://doi.org/10.1101/2024.01.26.577381.
[85] M. Cantini, H. Donnelly, M. J. Dalby, M. Salmeron-Sanchez, *Adv. Healthcare Mater.* **2020**, *9*, 1901259.
[86] M. Hu, Y. Li, J. Huang, X. Wang, J. Han, *ACS Appl. Bio Mater.* **2021**, *4*, 1340.
[87] H. Eslami Amirabadi, J. M. Donkers, E. Wierenga, B. Ingenhut, L. Pieters, L. Stevens, T. Donkers, J. Westerhout, R. Masereeuw, I. Bobeldijk-Pastorova, I. Nooijen, E. van de Steeg, *Lab Chip* **2021**, *22*, 326.
[88] R. Kim, J. H. Sung, *Adv. Healthcare Mater.* **2024**, *13*, 2302777.
[89] M. B. Esch, H. Ueno, D. R. Applegate, M. L. Shuler, *Lab Chip* **2016**, *16*, 2719.
[90] U. Marx, T. Akabane, T. B. Andersson, E. Baker, M. Beilmann, S. Beken, S. Brendler-Schwaab, M. Cirit, R. David, E. M. Dehne, I. Durieux, L. Ewart, S. C. Fitzpatrick, O. Frey, F. Fuchs, L. G. Griffith, G. A. Hamilton, T. Hartung, J. Hoeng, H. Hogberg, D. J. Hughes, D. E. Ingber, A. Iskandar, T. Kanamori, H. Kojima, J. Kuehnl, M. Leist, B. Li, P. Loskill, D. L. Mendrick, *ALTEX* **2020**, *37*, 364.
[91] H. J. Kim, D. Huh, G. Hamilton, D. E. Ingber, *Lab Chip* **2012**, *12*, 2165.
[92] M. Kasendra, A. Tovaglieri, A. Sontheimer-Phelps, S. Jalili-Firoozinezhad, A. Bein, A. Chalkiadaki, W. Scholl, C. Zhang, H.

Rickner, C. A. Richmond, H. Li, D. T. Breault, D. E. Ingber, *Sci. Rep.* **2018**, *8*, 2871.

[93] A. Apostolou, R. A. Panchakshari, A. Banerjee, D. V. Manatakis, M. D. Paraskevopoulou, R. Luc, G. Abu-Ali, A. Dimitriou, C. Lucchesi, G. Kulkarni, T. I. Maulana, M. Kasendra, J. S. Kerns, B. Bleck, L. Ewart, E. S. Manolakos, G. A. Hamilton, C. Giallourakis, K. Karalis, *CMGH* **2021**, *12*, 1719.

[94] M. Ballerini, S. Galiè, P. Tyagi, C. Catozzi, H. Raji, A. Nabinejad, A. D. G. Macandog, A. Cordiale, B. I. Slivinschi, K. K. Kugiejko, M. Freisa, P. Occhetta, J. A. Wargo, P. F. Ferrucci, E. Cocorocchio, N. Segata, A. Vignati, A. Morgun, M. Deleidi, T. Manzo, M. Rasponi, L. Nezi, *Nat. Biomed. Eng.* **2025**, *9*, 967.

[95] M. Nikolaev, O. Mitrofanova, N. Broguiere, S. Geraldo, D. Dutta, Y. Tabata, B. Elci, N. Brandenberg, I. Kolotuev, N. Gjorevski, H. Clevers, M. P. Lutolf, *Nature* **2020**, *585*, 574.

[96] E. E. Marr, T. J. Mulhern, M. Welch, P. Keegan, C. Caballero-Franco, B. G. Johnson, M. Kasaian, H. Azizgolshani, T. Petrie, J. Charest, E. Wiellette, *Sci. Rep.* **2023**, *13*, 8922.

[97] A. Marrella, P. Buratti, J. Markus, G. Firpo, M. Pesenti, T. Landry, S. Ayehunie, S. Scaglione, H. Kandarova, M. Aiello, *ALTEX* **2020**, *37*, 255.

[98] I. Maschmeyer, A. K. Lorenz, K. Schimek, T. Hasenberg, A. P. Ramme, J. Hübner, M. Lindner, C. Drewell, S. Bauer, A. Thomas, N. S. Sambo, F. Sonntag, R. Lauster, U. Marx, *Lab Chip* **2015**, *15*, 2688.